On-Chip Screening of Experimental Conditions for the Synthesis of Noble-Metal Nanostructures with Different Morphologies

*Jianhua Zhou, Jie Zeng, Jennifer Grant, Hongkai Wu, and Younan Xia**

The applications of nanostructures critically depend on their morphologies. Although significant progress has been made in the chemical synthesis of nanostructures with a variety of different morphologies, it is still highly desired to develop an approach that allows one to quickly identify the best set of parameters for nanostructure syntheses. Herein, an on-chip approach to the rapid screening of experimental conditions pivotal to the production of nanostructures with different morphologies is reported. The key component of this approach is an array of reactors containing solutions with a one- or two-dimensional gradient in reagent concentration, pH value, or reaction temperature. In the proof-of-concept experiments, the parameters needed for the production of Au and Pd nanostructures with various morphologies are quickly identified. In principle, this approach can be extended to other systems for rapid screening and optimization of experimental conditions involved in the syntheses of different types of nanostructures.

1. Introduction

Noble-metal nanostructures play important roles in many applications, including electronics, photonics, plasmonics, information storage, catalysis, and biomedicine.[1–9] Most of these applications critically rely on our ability to produce nanostructures with well-controlled and different morphologies. Over the past decade, solution-phase synthesis has emerged as probably the most productive and versatile route to noble-metal nanostructures with a wide variety of morphologies ranging from spheres to cubes, octahedrons, pyramids, plates, bars, rods, wires, cages, tubes, and multipods.[10–15] Meanwhile, it has also become clear that the final morphology taken by a nanostructure is highly sensitive to the reaction conditions, such as reagent concentration, pH value, temperature, and humidity, thus making it a challenging task to develop and/or optimize a synthesis protocol. Since most of the reported protocols were developed with a traditional trial-and-error and batch-based approach, the daunting demand on both time and materials only allows one to test a rather limited range of values for each experimental parameter. As a result, most of the published protocols do not necessarily operate under the optimal conditions, and there is an urgent need to develop a simple, inexpensive, and green approach that allows one to quickly identify the best set of parameters for generating nanostructures with a specific morphology.

Microfluidics, an emerging technology that works with very small volumes of reagents and allows one to run reactions in parallel, offers an ideal platform for high-throughput screening of experimental conditions.[16–19] For example, Ismagilov and co-workers have designed the SlipChip to perform multiplexed microfluidic reactions in glass without pumps or valves.[19,20] Combined with in situ analysis (e.g., X-ray diffraction), the SlipChip has been demonstrated as a powerful platform for screening of conditions for protein crystallization. Quake and co-workers have also developed a high-throughput pyrosequencing technology for analyzing

Dr. J. Zhou,[+] Dr. J. Zeng,[+] J. Grant, Prof. Y. Xia
Department of Biomedical Engineering
Washington University
St. Louis, MO 63130, USA
E-mail: xia@biomed.wustl.edu
Dr. J. Zhou, Prof. H. Wu
Department of Chemistry
The Hong Kong University of Science and Technology
Clear Water Bay, Kowloon, Hong Kong, P.R. China
[+] These authors contributed equally to this work.

DOI: 10.1002/smll.201101299

NANO MICRO small

antibody sequence.[21] By taking advantage of microfluidics, herein we present an on-chip technique that has the potential for rapid screening of experimental conditions pivotal to the production of nanostructures with different morphologies. This technique operates by running a large number of similar reactions in parallel with an on-chip array of miniature reactors, where a specific parameter of interest varies as a one- or two-dimensional gradient across the array. The use of a gradient allows us to simultaneously and quickly evaluate the parameter over a broad range of values in one single experiment.[22–25] It also enables the discovery of novel morphologies that tend to form under extreme conditions often missed by conventional batch-based syntheses as they typically operate on the basis of a few discrete data points.

2. Results and Discussion

Figure 1a shows a schematic of the procedure for fabricating an array of miniature reactors (see Figure S1 in the Supporting Information for details).[26–29] Briefly, two blocks of polydimethylsiloxane (PDMS) containing cylindrical holes were aligned and stacked on a silicon substrate to form a two-dimensional array of reactors. While the holes in the bottom PDMS block (1) contained reagent A with a concentration gradient, the holes in the top PDMS block (2) contained all other reagents with uniform concentrations across the entire library. To establish a concentration gradient for reagent A, a completely perforated PDMS block was sandwiched between a silicon substrate (3) and an agar hydrogel slab (4), as shown in Figure 1b.[30] The hydrogel slab contained two reservoirs: the one on the right-hand side was left empty while the one on the left was filled with a concentrated solution of reagent A. As such, reagent A would transport through the hydrogel slab from left to right, thereby establishing a gradient of A inside the hydrogel slab, as well as across different columns of the arrayed holes (Figure S2 in the Supporting Information). Uniform aliquots of reagent B, containing all other ingredients for the synthesis, were added to an array of holes partially perforated in the surface of block 2, which was then flipped over, placed on top of block 1, and aligned to allow the solutions in each reactor to mix and react. After reaction, the nanostructures formed in each reactor were naturally deposited on the silicon substrate (at the original site of the reactor) for characterization by scanning electron microscopy (SEM).

In the first demonstration, we focused on the synthesis of Au nanostructures due to their applications in fundamental investigation, device fabrication, and biomedical research.[31–35] The synthesis involves the mixing of an aqueous $HAuCl_4$ solution with an aqueous solution of cetyltrimethylammonium bromide (CTAB) to form a complex.[36–38] Subsequent addition of an aqueous solution of L-ascorbic acid reduces Au^{III} in the complex to Au^{I}, thereby generating a new complex.[36] The reduction is halted at the Au^{I} state until the addition of NaOH,[39] which can increase the pH of the solution and thus boost the reducing power of L-ascorbic acid to further reduce Au^{I} to elemental Au^{0}. In this system, we can manipulate the reaction kinetics by varying the concentration of NaOH, in an effort to generate Au nanostructures with potentially different morphologies.

As shown in Figure S1d in the Supporting Information, each PDMS block contained a 9×9 array of cylindrical holes 500 μm in diameter. One of the blocks was 500 μm thick and contained a gradient of NaOH concentration from 0 to 20 mM and the other had a thickness of 0.5 cm and held the same aqueous solution containing 0.25 mM $HAuCl_4$, 20 mM CTAB, and 1 mM L-ascorbic acid. The holes in the two PDMS blocks were aligned and brought together to form an array of miniature reactors. The reaction was conducted for 12 h at room temperature and under saturated humidity. After the reactors had been washed with water and dried, the Au

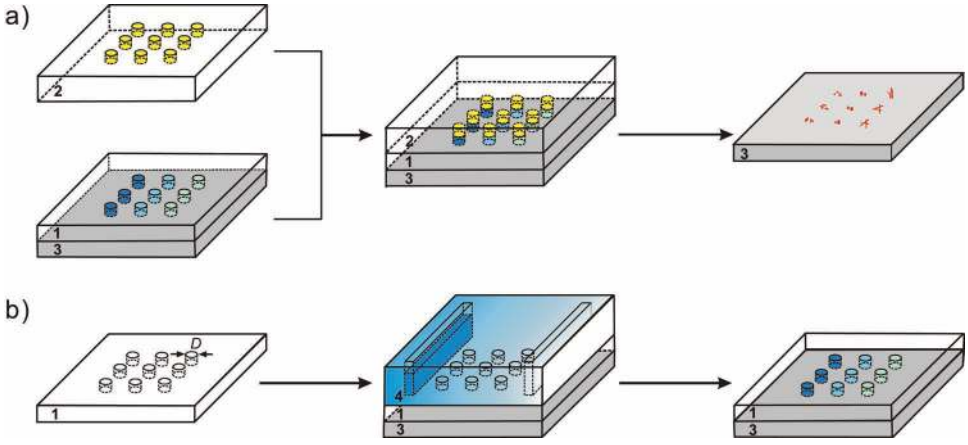

Figure 1. Procedure for fabricating an array of reactors on a Si substrate. a) A PDMS block (1) completely perforated with cylindrical holes contained a reagent of interest with a gradient in concentration. The wells in a partially perforated PDMS block (2) contained identical solutions of all other reagents involved in the synthesis. The reaction was initiated when the solutions in blocks 1 and 2 were mixed. After synthesis, blocks 1 and 2 were removed, leaving behind the nanostructures at the same sites of the Si substrate (3) for characterization. b) Formation of a concentration gradient for a reagent across the array of holes of the completely perforated PDMS block. A concentrated solution of the reagent was loaded into the left reservoir of the hydrogel slab (4) and allowed to diffuse towards the empty reservoir on the right-hand side. A gradient of the reagent was established across the hydrogel slab from left to right, as well as different columns of the arrayed holes.

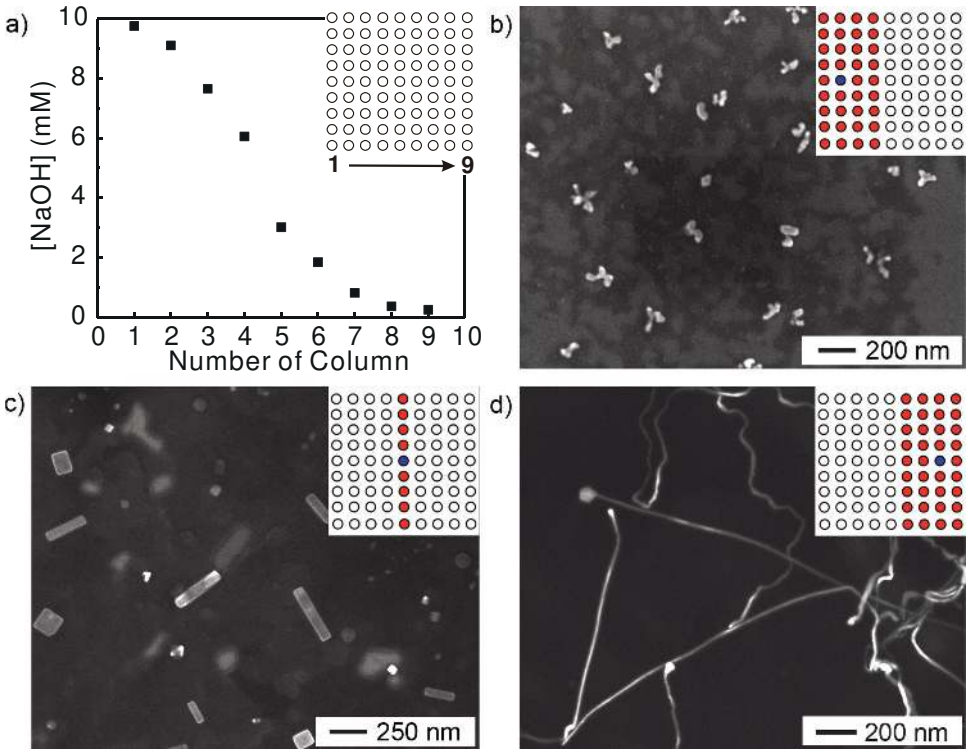

Figure 2. On-chip screening of NaOH concentration for the synthesis of Au nanostructures. a) Plot of NaOH concentrations in different columns of an array of reactors. The concentration of NaOH decreased from 10 to 0 mM when measured from the first to the last column of the array. The inset shows a schematic of the arrayed reactors, with the arrow indicating columns from 1 to 9. b–d) SEM images of Au nanostructures observed in a typical on-chip screening experiment: b) in columns 1–4, c) in column 5, and d) in columns 6–9. The inset shows a schematic of the arrayed reactors, with the blue spot indicating the specific reactor from which the corresponding SEM image was taken.

nanostructures remaining on the Si substrate were directly characterized by SEM.

The plot in **Figure 2**a shows the concentrations of NaOH in different columns of the two-dimensional array of holes. The NaOH concentration was determined by drawing an aliquot of the solution from each hole and quantifying the amount of sodium by ion chromatography (see the Experimental Section in the Supporting Information). Figure 2b–d shows SEM images of Au nanostructures formed in the array of reactors, which correspond to three different ranges of NaOH concentration. At relatively high concentrations of NaOH (10.0–5.8 mM, columns 1–4, marked in red), the products were dominated by irregularly shaped particles 20–100 nm in size (Figure 2b; the sample was taken from the reactor marked in blue). At moderate concentrations of NaOH (around 3.0 mM, column 5), we observed both Au nanocubes and nanobars (Figure 2c). At low concentrations (below 2.0 mM, columns 6–9), we observed a completely new morphology for Au nanostructures—wavy nanowires 20–30 nm in diameter and up to 100 μm in length (Figure 2d). As shown in Figure S3 in the Supporting Information, the products in different reactors from the same column displayed essentially the same morphology, thus indicating the uniformity in NaOH concentration in the same column of reactors.

The morphologies observed for the Au nanostructures correlated well with the reaction kinetics. For reactors in columns 1–4, high concentrations of NaOH corresponded to rapid reduction from Au^{I} to Au^{0}, which produced a large quantity of Au atoms in the solution. The plentiful supply of Au atoms would promote growth of thermodynamically favorable structures such as irregular nanoparticles. These structures typically contain multiply twinned defects and large proportions of {111} facets on the surface, and were favorable due to their low surface energy. In contrast, the low concentration of NaOH in reactors of columns 6–9 made L-ascorbic acid a rather weak reducing agent, greatly slowing down the reaction and shifting the growth into a kinetically controlled process. As a result, wavy nanowires not favored by thermodynamics were formed.[40] It is not unreasonable to expect that any successful synthesis of nanocubes and nanobars would require an intermediate reduction rate to balance the thermodynamic and kinetic effects and thus generate nanostructures belonging to neither growth mode. In comparison with the syntheses of Au irregular nanoparticles and nanowires, the formation of nanocubes and nanobars in reactors of column 5 was most sensitive to NaOH concentration and only worked within a very narrow range of NaOH concentrations.

Based on the results of this screening experiment, we also scaled up the syntheses from ≈200 nL for the on-chip reactors to 4.0 mL with conventional glass vials. In a typical set of syntheses, 2 mL of aqueous NaOH solutions with concentrations of 16, 6, and 0.5 mM were added, respectively, to 2 mL aqueous solutions containing 0.25 mM $HAuCl_4$, 20 mM

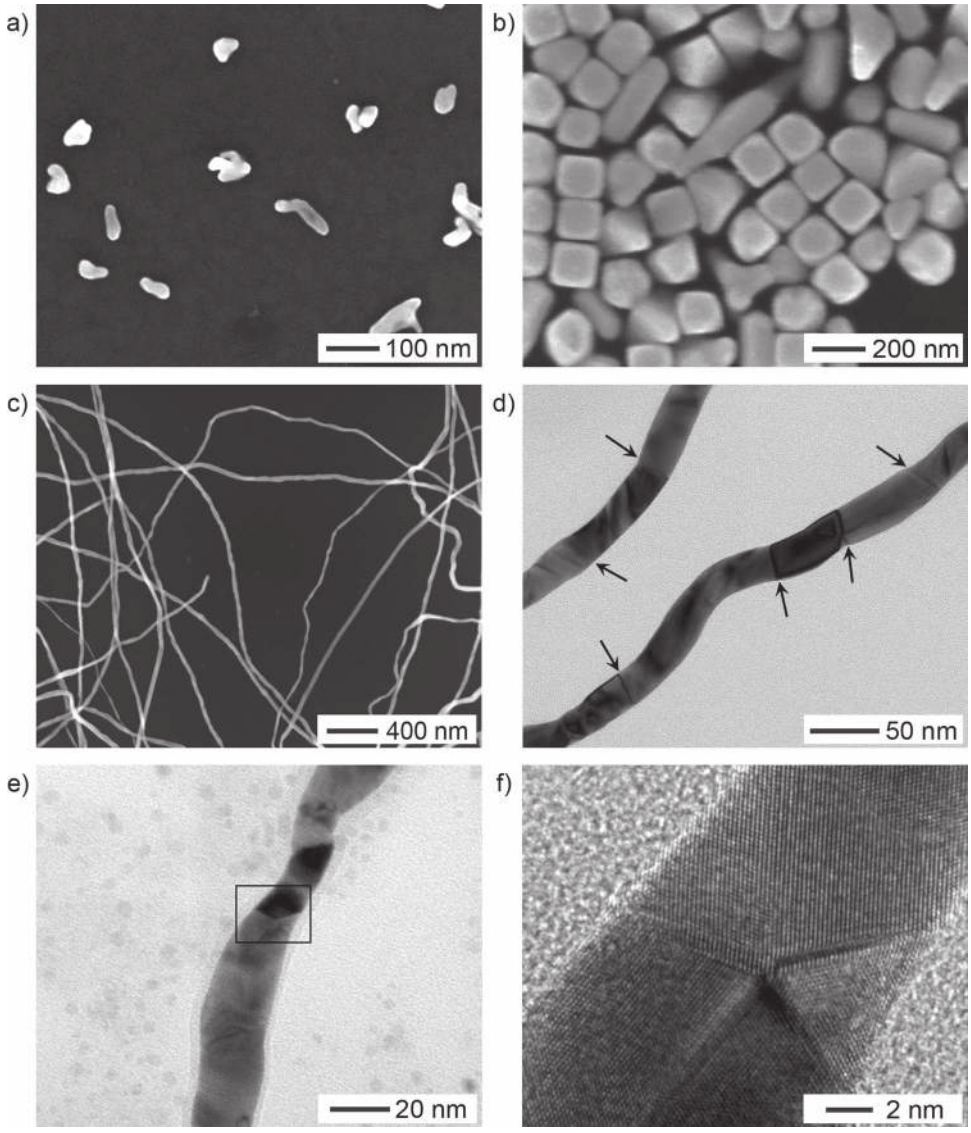

Figure 3. Scale-up syntheses of Au nanostructures from 200 nL (in the on-chip reactors) to 4.0 mL (in glass vials). a–c) SEM images showing Au nanostructures obtained with the NaOH concentrations being set to a) 8 mM, b) 3 mM, and c) 0.25 mM. d) Transmission electron microscopy (TEM) image of the wavy nanowires shown in (c), with the arrows indicating the boundaries of crystal domains. e,f) High-resolution TEM images of a Au wavy nanowire, where a penta-twinned defect structure can be clearly observed.

CTAB, and 1 mM L-ascorbic acid hosted in different glass vials. The solutions were mixed and then kept undisturbed, thus allowing the reactions to continue at room temperature for 12 h. **Figure 3**a–c shows typical SEM images of the as-prepared Au nanostructures. We obtained Au irregular nanoparticles, nanocubes and nanobars, and wavy nanowires, respectively, at NaOH concentrations of 8, 3, and 0.25 mM. It should be emphasized that the morphologies of the nanostructures in all the scale-up syntheses matched well with the screening experiments, thereby confirming the fidelity and reliability of our screening technique.

We also conducted TEM and high-resolution TEM studies to resolve the detailed structure of wavy nanowires. As shown in Figure 3d, we can clearly observe crystal domains and their boundaries, thus indicating that the wavy nanowires were polycrystalline. In addition, high-resolution TEM analysis indicates that the wavy nanowire also contained penta-twinned defects (see Figure 3f). Energy-dispersive X-ray (EDX) spectroscopy confirmed that these nanowires were made of pure Au (Figure S4 in the Supporting Information). It should be noted that the wavy nanowires obtained in both screening and scale-up syntheses were different from the previously reported Au nanowires, which were all straight and single crystals.[36–38,41–43] This result further demonstrates that our technique is able to screen and identify reaction conditions for generating new morphologies previously missed by conventional synthetic methods. The polycrystalline, wavy nanowires could only be obtained at extremely low NaOH concentrations. In a conventional batch-based synthesis such a low concentration of NaOH and thus exceptionally slow reaction rate would discourage anyone from spending the time and resources on this kind of test. In a screening experiment

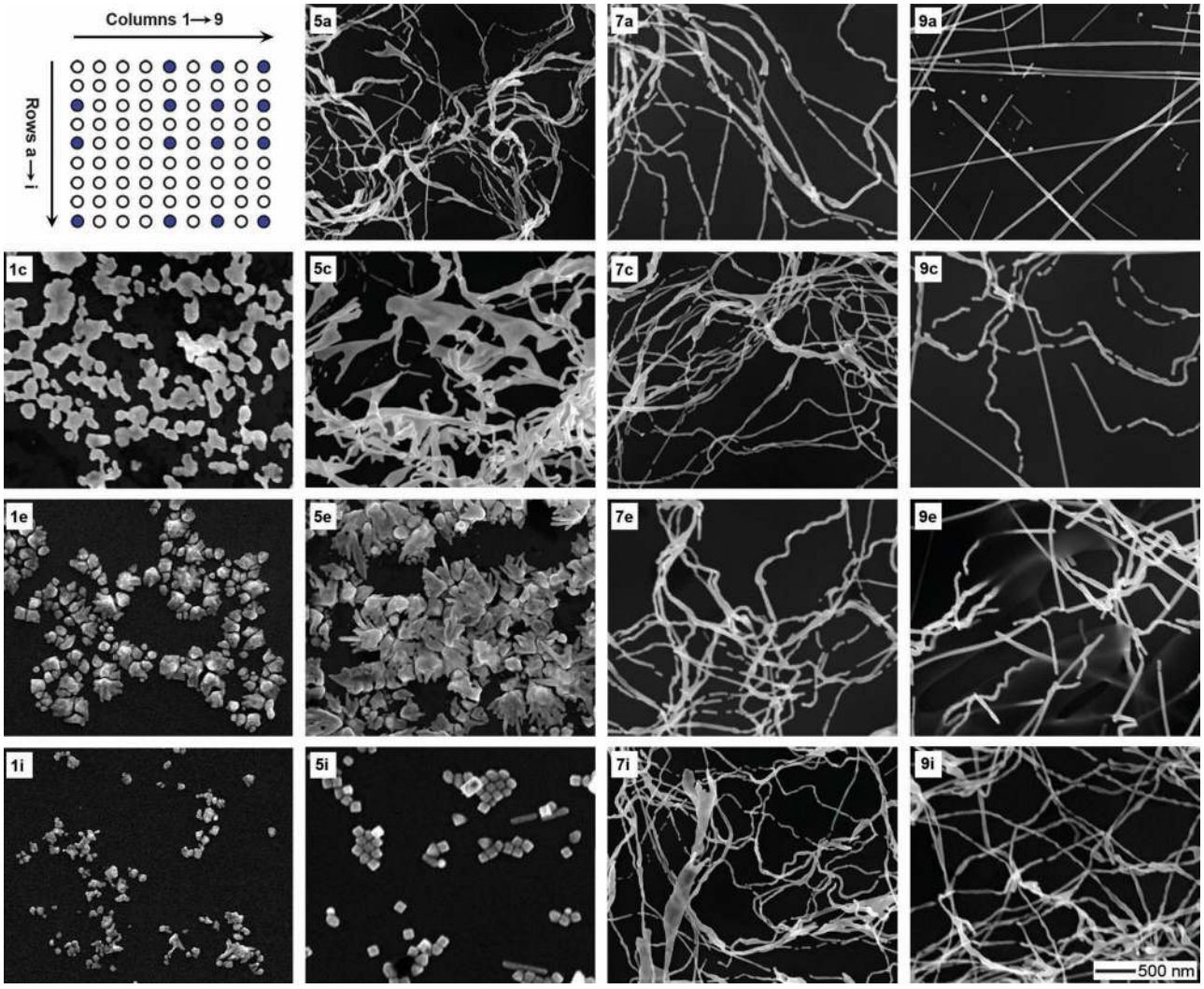

Figure 4. SEM images of Au nanostructures that were formed in a two-dimensional array of reactors with orthogonal gradients for the concentrations of NaOH and CTAB, respectively. For columns 1 to 9 (left to right), the NaOH concentration decreased from 10 to 0.2 mM; for rows a to i (top to bottom), the CTAB concentration decreased from 60 to 10 mM. Arrows indicate the directions along which the concentrations were reduced. Blue spots indicate the reactors from which the samples were taken for the corresponding SEM images. The scale bar in (9i) also applies to other SEM images.

with concentration gradient, however, such an extreme condition is naturally included in the test.

In a preliminary study, we also fabricated a chip with orthogonal concentration gradients for two different reagents to simultaneously evaluate their impacts on the morphologies of Au nanostructures (Figure S5 in the Supporting Information). Specifically, we established orthogonal concentration gradients for both CTAB and NaOH in a two-dimensional 9×9 array of reactors. The top-left panel of **Figure 4** shows a schematic of the arrayed reactors, with the arrows indicating columns from 1 to 9 (left to right, the NaOH concentration decreasing from 10 to 0.2 mM) and rows from a to i (top to bottom, the CTAB concentration decreasing from 60 to 10 mM). The concentrations of both CTAB and NaOH were determined by drawing an aliquot of the solution from each hole and quantifying the amount of bromide and sodium ions by ion chromatography. The other panels of Figure 4 show SEM images of Au nanostructures formed in the array of reactors, which correspond to four different ranges of NaOH and CTAB concentrations.

In addition to the irregular nanoparticles, nanocubes, and wavy nanowires observed in the one-dimensional gradient system, we obtained two other new morphologies at relatively high concentrations of CTAB—kites and straight nanobelts (see Figure S6 in the Supporting Information for TEM and high-resolution TEM images of the straight nanobelts).[44] The overall results are summarized in **Figure 5**. The morphologies observed in the two-dimensional screening experiments also correlated well with the reaction kinetics. For rows h and i, the screening results associated with the concentration of CTAB are consistent with the observations in Figure 2. For rows a and b, the concentration of CTAB was relatively high. The $AuCl_4^-$ precursor should be transformed to $AuCl_{4-x}Br_x^-$ due to a much larger stability constant for $AuBr_4^-$ relative to $AuCl_4^-$.[45] The reduction potential of $AuBr_4^-$/Au (0.854 V vs. reversible hydrogen electrode, RHE) is lower than that of

small NANO MICRO

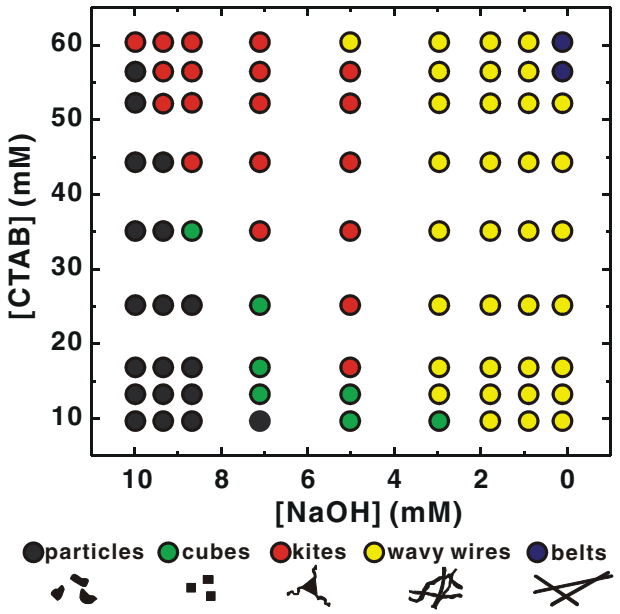

Figure 5. Diagram showing the correlations between the morphologies of the products in different reactors and the concentrations of NaOH and CTAB in a two-dimensional gradient system.

$AuCl_4^-$/Au (1.002 V vs. RHE).[45] As a result, the reduction of Au precursor is expected to be slowed down in the presence of excess Br^- ions, ultimately leading to a kinetically controlled process. In this case, those morphologies unfavorable with respect to thermodynamics, including nanobelts with parallel stacking faults (Figure S6), wavy nanowires, and kites (which might be an intermediate structure between wavy nanowires and nanoplates), are expected to dominate the products. It is also anticipated that intermediate concentrations of CTAB (for rows c–g) result in intermediate reduction rates for the Au precursor, and thus intermediate morphologies between those obtained at low and high concentrations of CTAB.

Besides screening of reagent concentrations and pH values, we also extended the on-chip technique to quickly screen the reaction temperatures for syntheses of nanostructures with different morphologies. To demonstrate this concept, we fabricated an on-chip system with uniform reagent concentrations but a gradient in temperature to examine the effect of this parameter on the morphology of Pd nanostructures. **Figure 6** shows photographs of a flat aluminum plate on which a temperature gradient was established by pumping cold (0.5 °C) water through one channel and hot (90.0 °C) water through another channel at the opposite side. A weight of 100 g was placed on top of the reactors to achieve good contact between the silicon substrate of the arrayed reactors and the aluminum plate. As shown in **Figure 7**a, the temperature increased from 33 to 76 °C across the nine columns of arrayed reactors. Figure 7b–d shows SEM images of representative Pd nanostructures formed in the array of reactors, which correspond to three different temperature ranges. Specifically, at temperatures below 40 °C (corresponding to columns 1 and 2), the products were dominated by Pd multipods (Figure 7b and Figure S7 in the Supporting Information, from the reactor marked in blue). At moderate temperatures ranging from 40 to 65 °C (columns 3–7), the products mainly contained triangular Pd nanoplates with truncations at the corners (Figure 7c). At relatively high temperatures in the range of 65–76 °C, we obtained uniform Pd nanocubes

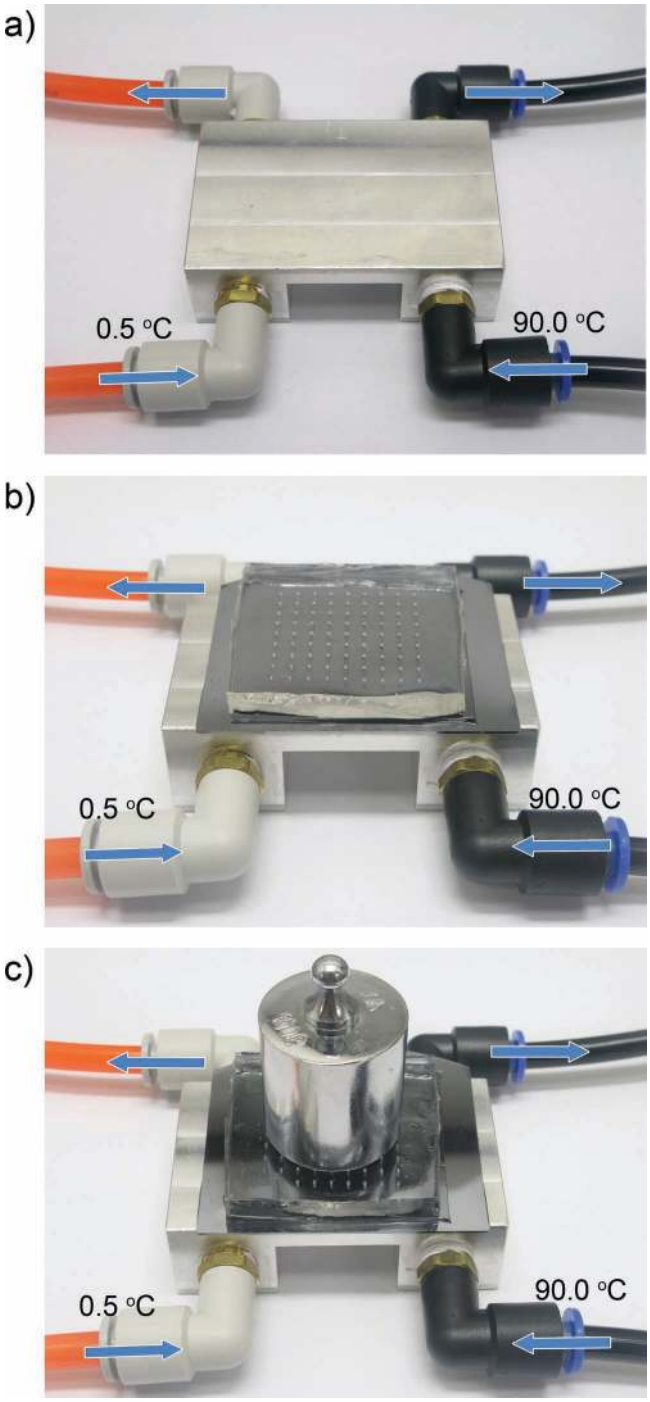

Figure 6. Photographs illustrating an on-chip system for screening the temperature of a synthesis. a) A flat aluminum plate with two channels on opposite sides. A temperature gradient was created on the surface of the plate by pumping cold (0.5 °C) water through the left channel and hot (90.0 °C) water through the right channel. b) An array of reactors supported on a silicon substrate that was placed on top of the aluminum plate. c) A weight of 100 g was applied to ensure a good contact between the silicon substrate and the plate.

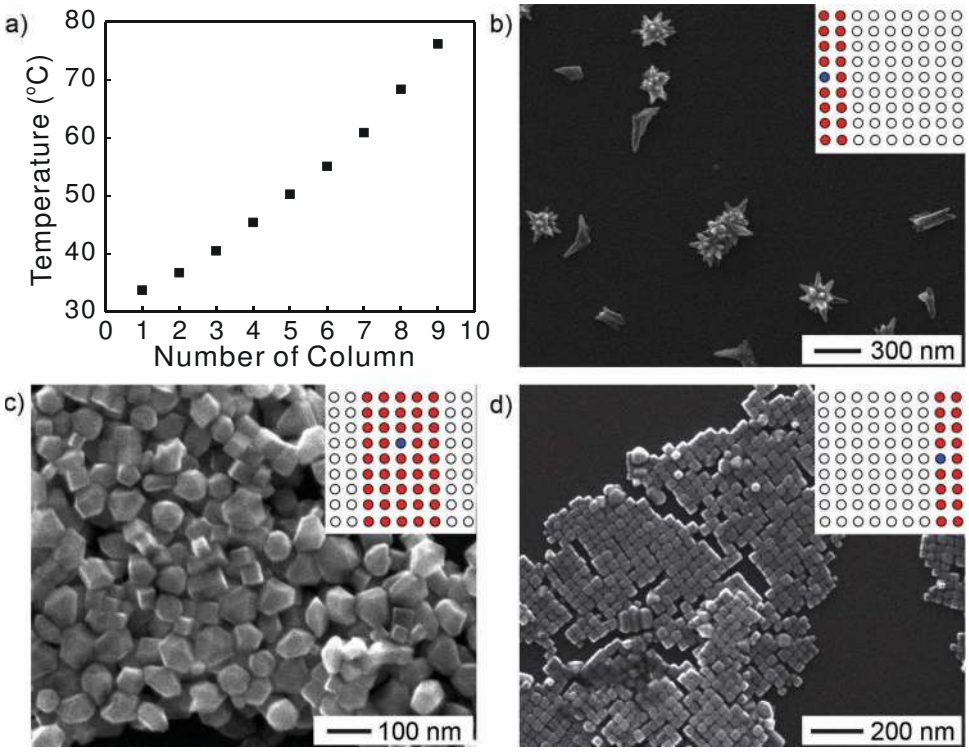

Figure 7. On-chip screening of temperature for the synthesis of Pd nanostructures. a) Distribution of temperature in different columns of the arrayed reactors. The temperature increased from 33 to 76 °C when measured from the first to the last column of the reactors. b–d) SEM images of Pd nanostructures observed in a temperature screening experiment: b) in columns 1 and 2, c) in columns 3–7, and d) in columns 8 and 9 with corresponding temperatures shown in (a). The inset shows a schematic of the arrayed reactors, with the blue spot indicating the specific reactor from which the corresponding SEM image was taken.

30–50 nm in edge length (Figure 7d). We also scaled up the syntheses with data from the screening experiments, and consistent morphologies were observed in all cases.

3. Conclusion

We have demonstrated an on-chip system as a general approach to rapid screening of reagent concentrations, pH values, and temperatures for syntheses of noble-metal nanostructures with different morphologies. By forming a gradient for each parameter, we could perform a large number of reactions in parallel over a broad range of values for the parameter to quickly identify the necessary condition for generating nanostructures with a specific morphology. This technique is expected to speed up the search for new and better synthetic protocols. Due to the use of very small amounts of reagents in each screening experiment, this on-chip platform is also expected to find use in optimizing the reaction conditions needed for high-volume production of nanostructures with different morphologies.

4. Experimental Section

Chemicals and Materials: Agarose, tridecafluoro-1,1,2,2-tetrahydrooctyl-1-trichlorosilane (TDFOCS), fluorescein sodium salt, gold(III) chloride trihydrate ($HAuCl_4 \cdot 3H_2O$), palladium(II) chloride ($PdCl_2$), cetyltrimethylammonium bromide (CTAB), L-ascorbic acid, and sodium hydroxide (NaOH) were all obtained from Sigma–Aldrich and used as received. Polydimethylsiloxane (PDMS) prepolymer (RTV615, a kit with components A and B) was obtained from Dow Corning (Midland, MI). The water used in all reactions was obtained by filtering through a set of Millipore cartridges (Epure, Dubuque, IA).

Fabrication of the Screening Chip: A PDMS mold, which was later used to fabricate a completely perforated PDMS block (1) and partially perforated PDMS block (2), was fabricated by molding against a poly(methyl methacrylate) (PMMA) plate with 9×9 wells. The diameter and depth of the wells were both 500 μm. The distance between the centers of two adjacent wells was 3 mm. Briefly, a PDMS prepolymer mixture (A:B = 10:1) was poured onto the PMMA plate, degassed, and then cured at 70 °C for 30 min, thereby generating a PDMS mold with dimensions 4×4 cm^2. The PDMS mold, now containing posts on the surface, was peeled off, treated with plasma for 90 s, and then exposed to TDFOCS vapor in a vacuum desiccator prior to use.

The PDMS block with an array of completely perforated holes was fabricated using soft lithography as described previously.[26,28] A PDMS prepolymer mixture was poured onto the PDMS mold, and a silicon wafer pretreated with TDFOCS was placed on top of the mixture. Pressure was applied to remove the excess prepolymer mixture. After curing at 70 °C for 30 min, the solidified PDMS block (like a membrane) was peeled off. The PDMS block, now bearing an array of completely perforated holes, was bonded to a clean silicon substrate (block 3) to generate an array of wells with silicon serving as the base.

small NANO MICRO

The PDMS block containing an array of partially perforated holes was fabricated in a similar manner using a greater volume of PDMS prepolymer mixture to produce a thicker block. Figure S1 in the Supporting Information shows schematic diagrams of the procedures for fabricating the PDMS mold, the completely perforated PDMS block on a silicon substrate, and the partially perforated PDMS block.

The hydrogel slab (block 4) was formed in a rectangular PDMS mold. Agarose powder was dissolved in deionized (DI) water at 150 °C to form a 1.0 wt% solution. The solution was then poured into the mold and allowed to cool and form a gel slab. The hydrogel slab had two reservoirs, one at each end. The thickness of the hydrogel slab was ≈3.0 mm. The two reservoirs were separated by ≈3.0 cm. The hydrogel slab was carefully transferred onto the PDMS block supported on a silicon substrate.

Generation of Concentration Gradient: We first used a molecular dye, fluorescein sodium salt, to demonstrate the formation of a stable chemical concentration gradient in a hydrogel slab, a key component of the screening technique. The gradient was generated by following the method described by Wu et al. with slight modifications.[30,46] Wu et al. reported that about 10 days were required to establish a concentration gradient over a distance of 3.0 cm within a hydrogel slab by diffusion only.[30] To speed up the process, we left one reservoir empty to take advantage of both concentration difference and hydraulic pressure difference between the two reservoirs and the evaporation of water to increase the diffusion rate. In the current setup, a stable gradient in fluorescein concentration could be established within 24 h. Figure S2 in the Supporting Information shows a fluorescence photograph of the fluorescein concentration gradient, which was also quantified by measuring the fluorescence intensity.

Screening of Reagent Concentrations for Syntheses of Au Nanostructures: A 20 mM NaOH solution was added to the left reservoir of the hydrogel slab. A stable NaOH concentration gradient was formed in the slab after 24 h of diffusion. Due to the hydrophilic nature of the silicon base which had been treated with plasma, the solution was drained into the wells in the PDMS block underneath the hydrogel slab, thereby filling the arrayed wells with NaOH solutions with different concentrations in a gradient.

In a typical synthesis, an aqueous solution of CTAB (0.5 mL, 40 mM) was mixed with an aqueous solution of $HAuCl_4$ (0.5 mL, 0.5 mM) at room temperature. Then a freshly prepared aqueous solution of L-ascorbic acid (0.05 mL, 20 mM) was quickly added to the solution under stirring. The solution became colorless and transparent within several seconds. This colorless solution was added to all wells of a PDMS block (2). After air bubbles in each well had been quickly removed under vacuum, a flat PDMS block was applied to the surface at an angle to wipe off the excess solution on the surface of the PDMS block.

The holes in the PDMS block with a uniform concentration were aligned with the wells in the PDMS block with a concentration gradient of NaOH, and brought into contact. Because both PDMS blocks were molded from the same template, they could be aligned perfectly to generate a good seal between them. Upon contact and mixing between the two solutions, Au nanostructures started to form and the reaction was allowed to continue overnight for 12 h under 100% humidity. By the end of the synthesis, the upper PDMS block was removed and the remaining system was dried under vacuum and then immersed in DI water for 24 h. After this purification step and drying, the bottom PDMS block was peeled off, thereby leaving behind Au nanostructures (at their original sites defined by the wells) on the silicon substrate for SEM characterization.

Scale-up Synthesis of the Au Nanostructures: Based on the screening results, the syntheses were scaled up from ≈200 nL to 4.0 mL. In a typical synthesis, 2 mL of NaOH solutions with concentrations of 16, 6, and 0.5 mM were added, respectively, to 2 mL solutions containing 0.25 mM $HAuCl_4$, 20 mM CTAB, and 1 mM L-ascorbic acid hosted in three glass vials. The solutions were mixed and allowed to react at room temperature for 12 h. Products were collected by centrifugation at 10 000 rpm for 10 min and washing with DI water. This procedure was repeated once, after which the particles were resuspended in DI water and dropped onto substrates for imaging.

Screening of Temperature for the Synthesis of Pd Nanostructures: An aluminum plate containing two channels on opposite sides was used to establish a temperature gradient (see Figure 6). Cold (0.5 °C) water was pumped through one of the channels while hot (90.0 °C) water was pumped through the other channel at a rate of 0.7 L min^{-1}. The temperature profile was recorded using a miniaturized negative temperature coefficient thermistor thermometer (TTF103, Kingwahoo Electronics Co., Dongguan, China). As shown in Figure 7a, a stable temperature gradient formed on the surface of the aluminum plate and across the array of reactors placed on top of the plate.

In a typical synthesis, an aqueous solution of CTAB (0.5 mL, 40 mM) was added to an aqueous solution of $PdCl_2$ (0.5 mL, 2.0 mM) at room temperature. This mixture was added to each hole of a partially perforated PDMS block. After air bubbles in each hole had been quickly removed under vacuum, a flat PDMS slab was applied to the surface at an angle to wipe off the excess solution on the surface of the PDMS block. Simultaneously, a freshly prepared aqueous solution of L-ascorbic acid (1.0 mL, 2.0 mM) was added to each hole of a completely perforated PDMS block supported on a silicon substrate. After air bubbles in each hole had been quickly removed under vacuum, a flat PDMS slab was applied to the surface at an angle to wipe off the excess solution on the surface of the PDMS block.

The holes in the partially perforated PDMS block were aligned with the holes in the partially perforated PDMS block and brought into contact face to face. The device was placed on top of the aluminum plate with a temperature gradient (with the silicon substrate in contact with the plate) and a weight of 100 g was placed on the top to maintain a good contact (Figure 6). The reactions were allowed to proceed for 6 min. To quench the reaction, the arrayed reactors supported on a silicon substrate were removed from the aluminum plate. By the end of the synthesis, the upper PDMS block was removed and the remaining system was dried under vacuum and then immersed in DI water for 24 h. After this purification step and drying, the bottom PDMS block was peeled off, thereby leaving behind Pd nanostructures (at their original sites defined by the wells) on the silicon substrate for SEM characterization.

Characterization: SEM images of Au nanostructures were taken using a Nova NanoSEM 2300 microscope equipped with an energy-dispersive spectrometer (FEI, Hillsboro, OR). TEM images were captured with a Tenai G2 Spirit Twin microscope operated at 120 kV (FEI, Hillsboro, OR). TEM samples were prepared by dropping a suspension of the nanostructures (sample from a different reactor) onto a piece of carbon-coated copper grid (Ted Pella,

Redding, CA). Ion chromatography data were obtained from a DX500 ion chromatography system (Dionex, Sunnyvale, CA). Fluorescence images were captured using a Power-Shot G9 digital camera, and the fluorescence intensities (shown in Figures S2 and S5, Supporting Information) were obtained from the fluorescence images using Image-Pro Plus 6.0 software.

Supporting Information

Supporting Information is available from the Wiley Online Library or from the author.

Acknowledgements

This work was supported in part by a research grant from the NSF (DMR-0804088) and startup funds from Washington University in St. Louis. J.Z. was partially supported by the Hong Kong RGC (604509 and N_HKUST617109). Y.X. was also partially supported by the World Class University (WCU) program through the National Research Foundation of Korea funded by the Ministry of Education, Science, and Technology (R32-20031). Part of the research was performed at the Nano Research Facility (NRF), a member of the National Nanotechnology Infrastructure Network (NNIN), which is funded by the NSF under award no. ECS-0335765.

[1] Y. Yin, R. M. Rioux, C. K. Erdonmex, S. Hughes, G. A. Somorjai, A. P. Alivisatos, *Science* **2004**, *304*, 711.
[2] R. Jin, Y. Cao, C. A. Mirkin, K. L. Kelly, G. C. Schatz, J. G. Zheng, *Science* **2001**, *294*, 1901.
[3] Y. Sun, Y. Xia, *Science* **2002**, *298*, 2176.
[4] E. Prodan, C. Radloff, N. J. Halas, P. Nordlander, *Science* **2003**, *302*, 419.
[5] J. Lee, P. Hernandez, J. Lee, A. O. Govorov, N. A. Kotov, *Nat. Mater.* **2007**, *6*, 291.
[6] S. Sun, C. B. Murray, D. Weller, L. Folks, A. Moser, *Science* **2000**, *287*, 1989.
[7] V. F. Puntes, K. M. Krishnan, A. P. Alivisatos, *Science* **2001**, *291*, 2115.
[8] T. S. Ahmadi, Z. L. Wang, T. C. Green, A. Henglein, M. A. El-Sayed, *Science* **1996**, *272*, 1924.
[9] D. V. Talapin, J. S. Lee, M. V. Kovalenko, E. V. Shevchenko, *Chem. Rev.* **2010**, *110*, 389.
[10] Y. Xia, Y. Xiong, B. Lim, S. E. Skrabalak, *Angew. Chem. Int. Ed.* **2009**, *48*, 60.
[11] B. L. Cushing, V. L. Kolesnichenko, C. J. O'Connor, *Chem. Rev.* **2004**, *104*, 3893.
[12] C. J. Murphy, T. K. Sau, A. M. Gole, C. J. Orendorff, J. Gao, L. Gou, S. E. Hunyadi, T. Li, *J. Phys. Chem. B* **2005**, *109*, 13857.
[13] Y. Yin, A. P. Alivisatos, *Nature* **2005**, *437*, 664.
[14] C. Burda, X. Chen, R. Narayanan, M. A. El-Sayed, *Chem. Rev.* **2005**, *105*, 1025.
[15] C. J. Murphy, N. R. Jana, *Adv. Mater.* **2002**, *14*, 80.
[16] G. M. Whitesides, *Nature* **2006**, *442*, 368.
[17] J. I. Park, A. Saffari, S. Kumar, A. Günther, E. Kumacheva, *Annu. Rev. Mater. Res.* **2010**, *40*, 415.
[18] J. Hong, J. B. Edel, A. J. deMello, *Drug Discov. Today* **2009**, *14*, 134.
[19] L. Li, R. F. Ismagilov, *Annu. Rev. Biophys.* **2010**, *39*, 139.
[20] W. Du, L. Li, K. P. Nichols, R. F. Ismagilov, *Lab Chip* **2009**, *9*, 2286.
[21] J. A. Weinstein, N. Jiang, R. A. White III, D. S. Fisher, S. R. Quake, *Science* **2009**, *324*, 807.
[22] B. A. Grzybowski, K. J. M. Bishop, C. J. Campbell, M. Fialkowski, S. K. Smoukov, *Soft Matter* **2005**, *1*, 114.
[23] G. Mahmud, K. J. M. Bishop, Y. Chegel, S. K. Smoukov, B. A. Grzybowski, *J. Am. Chem. Soc.* **2008**, *130*, 2146.
[24] T. M. Keenan, A. Folch, *Lab Chip* **2008**, *8*, 34.
[25] C. J. Bettinger, H. A. Becerril, D. H. Kim, B.-L. Lee, S. Lee, Z. Bao, *Adv. Mater.* **2011**, *23*, 1257.
[26] Y. Xia, G. M. Whitesides, *Angew. Chem. Int. Ed.* **1998**, *37*, 551.
[27] T. Thorsen, S. J. Maerkl, S. R. Quake, *Science* **2002**, *298*, 580.
[28] H. Yan, Y. Zhao, C. Qiu, H. Wu, *Sens. Actuators B* **2008**, *132*, 20.
[29] B. Huang, K. Wu, D. Bhaya, A. Grossman, S. Granier, B. K. Kobilka, R. N. Zare, *Science* **2007**, *315*, 81.
[30] H. Wu, B. Huang, R. N. Zare, *J. Am. Chem. Soc.* **2006**, *128*, 4194.
[31] M. C. Daniel, D. Astruc, *Chem. Rev.* **2004**, *104*, 293.
[32] M. Yang, R. Alvarez-Puebla, H.-S. Kim, P. Aldeanueva-Potel, L. M. Liz-Marzán, N. A. Kotov, *Nano Lett.* **2010**, *10*, 4013.
[33] X. Huang, I. H. El-Sayed, W. Qian, M. A. El-Sayed, *J. Am. Chem. Soc.* **2006**, *128*, 2115.
[34] R. Elghanian, J. J. Storhoff, R. C. Mucic, R. L. Letsinger, C. A. Mirkin, *Science* **1997**, *277*, 1078.
[35] L. R. Hirsch, R. J. Stafford, J. A. Bankson, S. R. Sershen, B. Rivera, R. E. Price, J. D. Hazle, N. J. Halas, J. L. West, *Proc. Natl. Acad. Sci. USA* **2003**, *100*, 13549.
[36] N. R. Jana, L. Gearheart, C. J. Murphy, *J. Phys. Chem. B* **2001**, *105*, 4065.
[37] B. Nikoobakht, M. A. El-Sayed, *Chem. Mater.* **2003**, *15*, 1957.
[38] A. Gole, C. J. Murphy, *Chem. Mater.* **2004**, *16*, 3633.
[39] S. Chen, Z. L. Wang, J. Ballato, S. H. Foulger, D. L. Carroll, *J. Am. Chem. Soc.* **2003**, *125*, 16186.
[40] M. A. Watzky, R. G. Finke, *J. Am. Chem. Soc.* **1997**, *119*, 10382.
[41] X. Lu, M. S. Yavuz, H.-Y. Tuan, B. A. Korgel, Y. Xia, *J. Am. Chem. Soc.* **2008**, *130*, 8900.
[42] C. Wang, Y. Hu, C. M. Lieber, S. Sun, *J. Am. Chem. Soc.* **2008**, *130*, 8902.
[43] Z. Huo, C. K. Tsung, W. Huang, X. Zhang, P. Yang, *Nano Lett.* **2008**, *8*, 2041.
[44] Y. Sun, B. Mayers, Y. Xia, *Nano Lett.* **2003**, *3*, 675.
[45] G. Inzelt, *Encyclopedia of Electrochemistry* (Eds: A. J. Bard, M. Stratmann, F. Scholz, C. J. Pickett), Wiley-VCH, Weinheim **2006**, p.46.
[46] J. He, Y. Du, J. L. Villa-Uribe, C. Hwang, D. Li, A. Khademhosseini, *Adv. Funct. Mater.* **2010**, *20*, 131.

Received: June 29, 2011
Published online: September 15, 2011

